Journal of Materials Chemistry

Cite this: *J. Mater. Chem.*, 2012, **22**, 4921

www.rsc.org/materials

PAPER

Large-scale production of ultrathin topological insulator bismuth telluride nanosheets by a hydrothermal intercalation and exfoliation route†

Long Ren, Xiang Qi,* Yundan Liu, Guolin Hao, Zongyu Huang, Xianghua Zou, Liwen Yang, Jun Li and Jianxin Zhong

Received 18th November 2011, Accepted 4th January 2012
DOI: 10.1039/c2jm15973b

A convenient hydrothermal intercalation/exfoliation method for large-scale manufacturing of bismuth telluride (Bi_2Te_3) nanosheets is reported here. Lithium cations can be intercalated between the layers of Bi_2Te_3 using the reducing power of ethylene glycol in the common hydrothermal process, and high quality Bi_2Te_3 nanosheets with thickness down to only 3–4 nm are obtained by removing lithium in the following exfoliating process. Scanning electron microscopy, transmission electron microscopy and Raman spectrum characterizations confirm that the high yield of Bi_2Te_3 nanosheets with good quality were successfully achieved and the sizes of the immense nanosheets reached 200 nm width and 1 μm length. This hydrothermal intercalation/exfoliation method is general, as it has been extended to other layered materials, such as Bi_2Se_3 and MoS_2. Our results suggest a simple route for the large-scale production of thin and flat Bi_2Te_3 nanosheets, which may be beneficial to further electronic and spintronics applications.

1. Introduction

Bismuth telluride (Bi_2Te_3) is a narrow energy gap semiconductor material with a hexagonal layered structure comprised of five atom thick covalently bonded stacks of Te–Bi–Te–Bi–Te within each layer with the sheets held together by van der Waals forces.[1] Bismuth telluride and its alloys are proposed to be the best thermoelectric materials because they possess the highest thermoelectric figure of merit known at room temperature.[2] Recently, research on Bi_2Te_3 has attracted much interest for it is predicted to be a three-dimensional (3D) topological insulator (TI), a new class of quantum matter with conductive massless Dirac fermions on the surface.[3] The robust and nontrivial metallic surface states induced by strong spin–orbit coupling of 3D TIs are topologically protected against back scattering from time-reversal invariant defects and impurities, promising realization of dissipationless electron transport in the absence of high magnetic fields.[4,5] Experimentally, bulk single crystals like Bi_2Te_3, Bi_2Se_3 and Sb_2Te_3, were confirmed by angle-resolved photoemission spectroscopy as 3D TIs with the existence of the spin-momentum locked Dirac fermion nature of the surface states.[6–9] Compared with bulk samples, nanostructured TI materials are a remarkable system for probing TI surface states for their large surface-to-volume ratio.[10] Meanwhile, TI nanostructures are not only expected to significantly enhance surface conduction, but also proposed to effectively manipulate the surface state or modulate the chemical potential by external means.[10–12] Therefore, synthesizing low-dimensional structures out of this family of compounds is desired for TI study. Currently, high-crystalline quality thin films of TI can be obtained by MBE growth,[13,14] but MBE is expensive and less accessible. Furthermore, vapor–liquid–solid growth has been shown to be an effective route to produce high quality nanoribbons and nanowires of chalcogenide materials with a moderate thickness range of 30–100 nm.[11,15,16] Cui and coworkers developed a catalyst-free vapor solid synthesis process to grow ultrathin nanoplates of Bi_2Se_3 and Bi_2Te_3 with thicknesses down to ~3 nm.[10] However, the migration and thickness uniformity of as-prepared nanomaterials are still problems. In view of the weak van der Waals interaction between the adjacent quintuple layers (one quintuple layer formed by five atom thick covalently bonded stacks of Te(Se)–Bi–Te(Se)–Bi–Te(Se)) of Bi_2Te_3 or Bi_2Se_3, mechanical exfoliation of thin sheets from bulk crystals, widely used for obtaining graphene from graphite,[17] can be also used to achieve thin TI layers.[18,19] Balandin and coworkers have used the mechanical exfoliation method to obtain good quality thin-film Bi_2Se_3 TI samples for related investigations.[20,21] However, this kind of method suffered from low yield and irregular shapes of products. Most recently, Coleman and co-workers made great effective efforts to disperse and exfoliate layered materials including Bi_2Te_3 in common solvents by sonication,[22] but the Bi_2Te_3 flakes exfoliated in that way were not flat and not thin enough for TI research. Moreover, the layered structure makes it possible to intercalate atoms like Cu or Li between connected quintuple layers and form nanomaterials by

Laboratory for Quantum Engineering and Micro-Nano Energy Technology and Faculty of Materials and Optoelectronic Physics, Xiangtan University, Hunan, 411105, P. R. China. E-mail: xqi@xtu.edu.cn

† Electronic supplementary information (ESI) available. See DOI: 10.1039/c2jm15973b

exfoliation.[23–28] Considering this feature, intercalation of layered Bi_2Te_3 by electrochemical methods using a lithium anode was originally attempted.[25,26] However, a very limited amount of Li intercalation of Bi_2Te_3 was achieved since partially intercalated pieces readily break off from the Bi_2Te_3 cathode during intercalation. Effective intercalation of Bi_2Te_3 and Bi_2Se_3 has been achieved by a chemical intercalation method, but it needed special reaction equipment to contain the extreme experimental conditions of a liquid ammonia atmosphere.[27,28] To overcome the problem of inconvenient experimental installation and exacting experimental conditions, here we demonstrate a new method to intercalate and exfoliate bulk Bi_2Te_3 using lithium solution *via* a common hydrothermal process. This novel chemical intercalation method helps us easily to achieve high levels of Li intercalation and superior yield of Bi_2Te_3 nanosheets *via* a simple exfoliation process, promising large-scale preparation and wide applications of TIs nanostructures in future spintronics devices.

2. Experimental section

2.1 Synthesis

In a typical synthesis, the Bi_2Te_3 bulk crystals (99.999%, Alfa Aesar) were placed into a 30 mL Teflon-lined autoclave filled with an ethylene glycol solution of lithium hydroxide (8 g L^{-1}). The autoclave was oven-heated at 200 °C for 24 h to achieve the intercalation of Bi_2Te_3 by the lithium ions (Li^+) dissolved in the solution. After Li intercalation, the dispersions in the solution were collected by filtration and rinsed with acetone to eliminate the excess ethylene glycol solution of lithium hydroxide. Colloidal suspensions of bismuth telluride can be readily prepared by exfoliating the lithiated powder in deionized water. By filtering through porous polyvinylidene fluoride (PVDF) (0.45 μm nominal pore size) membranes, the Bi_2Te_3 nanosheet membranes were obtained after drying at 60 °C. Samples for characterization could be collected from the membranes or directly dispersed in the ethanol.

2.2 Characterization

The morphologies of the large bulk Bi_2Te_3 and the as-synthesized nanosheets were characterized by using scanning electron microscopy (SEM, JEOL, JSM-6610LV) with energy dispersive spectroscopy (EDS). The microstructure of Bi_2Te_3 nanosheets was investigated by using transmission electron microscopy (TEM, JEOL JEM-3010) equipped with selected area electron diffraction (SAED). Raman spectra were collected for bulk samples and nanosheets of Bi_2Te_3 using a Horiba–Jobin–Yvon LabRam HR confocal microscope, excited at room temperature with laser light ($\lambda = 488$ nm). Atomic force microscopy (AFM, SPI-3800N) was used to measure the thickness of Bi_2Te_3 nanosheets as well as thin films formed by direct deposition on oxidized silicon (SiO_2).

3. Results and discussion

Fig. 1 illustrates the remarkable changes of the hydrothermal solution and the Bi_2Te_3 bulk before and after the reactions. As shown in Fig. 1 (b), the ethylene glycol solution of lithium hydroxide turns turbid after the hydrothermal reaction with respect to the former pellucid solution with a large piece of bulk Bi_2Te_3 in the bottom which is shown in Fig. 1 (a). Considering the lithium solution of the same consistency without the bulk Bi_2Te_3 was still clear after the hydrothermal process (digital image is provided in ESI,† Fig. S1), we suggest that the turbid solution was caused by the insertion of Li^+ ions into the bulk Bi_2Te_3. The surface of this large bulk piece of Bi_2Te_3 was characterized by SEM to gain insight into the alteration of the bulk Bi_2Te_3 before and after reaction. As shown by the SEM images in Fig. 1 (c) and (d), the original smooth and flat layered surface of the bulk Bi_2Te_3 became porous and roughened. Moreover, layered internal features were observed from the high-resolution image inserted in Fig. 1 (d). This phenomenon indicates that the macro-scaled Bi_2Te_3 bulk has been roughly broken down into nanoscale by Li intercalation, and the Li-intercalated small lithiated bismuth telluride units separated from the bulk have dispersed in the solution to form the turbid suspension. Moreover, the bulk materials dissolved completely into solution after intercalating for three days, confirming that a high level of intercalation has been achieved. Note that if larger bismuth telluride crystals are used, they must be ground to a fine powder before intercalation, otherwise some non-intercalated materials will remain, as shown in Fig. 1 (a, b).

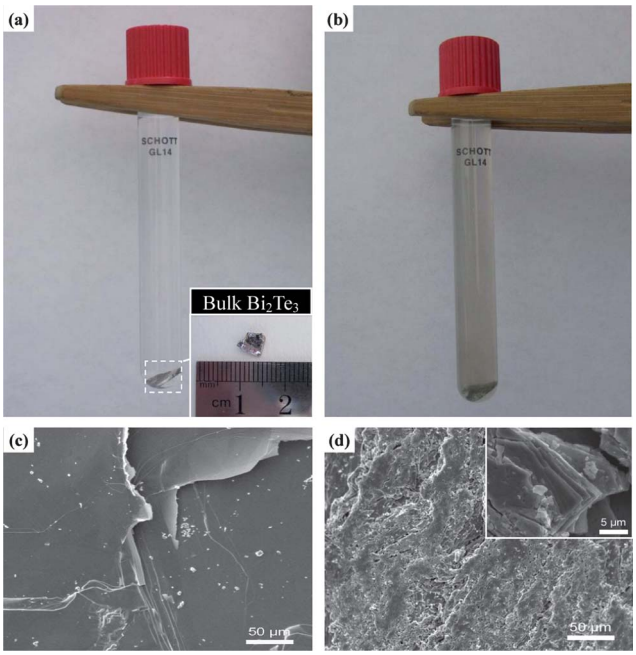

Fig. 1 Digital photos of the change in the solution (a) before and (b) after reaction (the image inserted in (a) is the morphology of a large piece of bulk Bi_2Te_3). SEM images of the bulk Bi_2Te_3 piece (c) before and (d) after reaction.

After Li-intercalation, the powder of Li-intercalated units was exposed to deionized water to make the Li atoms inside the interlayers react with water and explode like atom-scaled bombs. Fig. 2 (a) shows the SEM image of the as-produced powder, it can be clearly observed that large-scale isolated nanosheets with large lateral dimensions are widespread. As distinct from the nanoparticles produced by the electrochemical route in ref. 26, the products here are almost two-dimensional sheet-like structures with intact surface texture. The elemental composition and

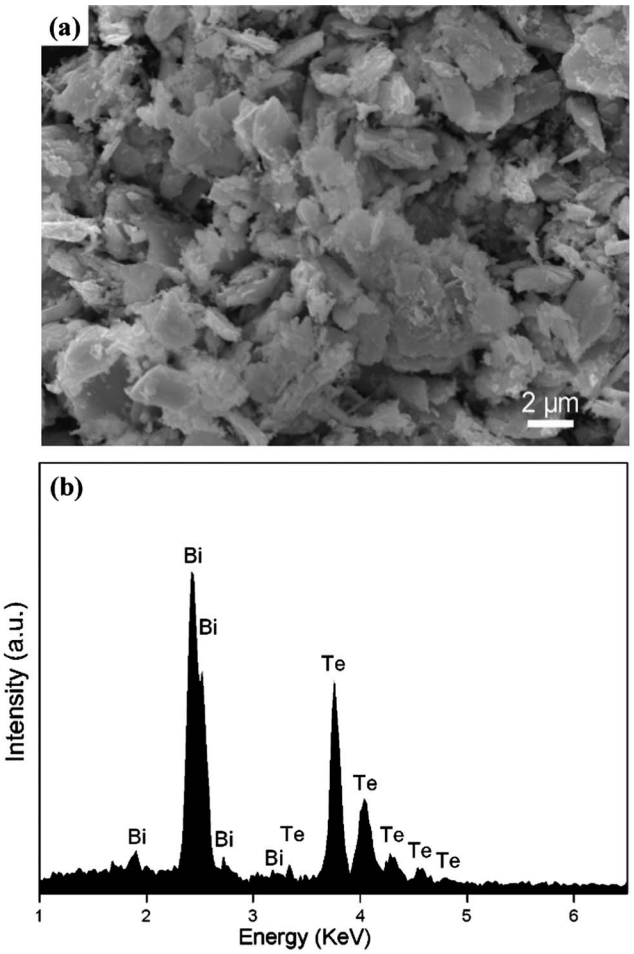

Fig. 2 (a) SEM image and (b) EDS analysis of the exfoliated Bi_2Te_3 nanosheets.

stoichiometry of as-prepared samples were further studied by EDS as shown in Fig. 2 (b). The analysis of the measured EDS spectrum of the sample gave molar percentages of Bi and Te of ~42.2% and 57.8%, respectively. Thus, the structural make up of the exfoliation has a 2 : 3 ratio of Bi to Te atoms (*e.g.*, Te-Bi-Te-Bi-Te), which corresponds to the Bi_2Te_3 formula.

Fig. 3 shows the typical high-magnification TEM images of an individual Bi_2Te_3 sheet which were characterized by TEM. It is clearly observed that the exfoliated material consisted of a very thin layer with a smooth surface. Fig. 3 (a) illustrates a large sheet with about 200 nm width and 1 μm length. Corresponding high-resolution TEM (HRTEM) lattice fringes and the SAED spot pattern, shown in Fig. 3 (b) and the inset image, demonstrate the single crystalline nature of the nanosheets. A HRTEM image reveals expected hexagonal lattice fringes with a lattice spacing of 0.22 nm, consistent with the lattice spacing of (1120) planes.

The Raman spectra of Bi_2Te_3 nanosheets and bulk Bi_2Te_3 as a reference are shown in Fig. 4. Bi_2Te_3 has 15 lattice vibration modes (phonon polarization branches), and twelve of those 15 branches are optical phonons while the remaining three are acoustic phonons. The 12 optical modes are classified into 2 A_{1g}, 2 E_g, 2 E_u, and 2 A_{1u}. The four Raman active modes E_g^1, A_{1g}^1, E_g^2, and A_{1g}^2 are observed in bulk crystalline Bi_2Te_3 at 40.2 cm^{-1},

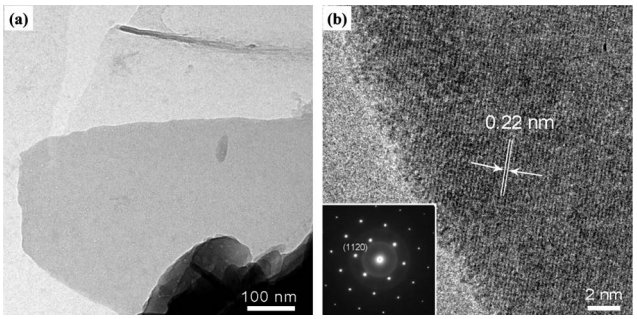

Fig. 3 (a) TEM image of exfoliated Bi_2Te_3 nanosheets transferred to a lacey carbon support film on a TEM copper grid; (b) HRTEM image obtained from the same Bi_2Te_3 nanosheet with the corresponding SAED pattern.

60.2 cm^{-1}, 100.8 cm^{-1}, and 133.2 cm^{-1}, respectively, which are consistent with the literature.[29–31] Each of the E_g and A_{1g} modes is 2-fold degenerate: in E_g, the atoms vibrate in the basal plane, while in A_{1g}, the atoms vibrate along c_H.[29] The measured intensity of in-plane vibrations $I(E_g^2)$ is higher than that of the out-of-plane vibrations $I(A_{1g}^2)$, which is also in agreement with literature for bulk Bi_2Te_3.[29–31] These four modes are also observed in the as-prepared Bi_2Te_3 nanosheets and the peak intensity typically becomes stronger due to the decrease in thickness of exfoliated Bi_2Te_3 flakes.[32,33] Interestingly, an additional strongest peak, identified as A_{1u}, appears in the Raman spectrum of the as-prepared Bi_2Te_3 nanosheets. The A_{1u} peak (which is the infrared-active mode in bulk crystalline Bi_2Te_3) is likely to become Raman active due to the symmetry breaking in atomically thin films.[31] In concrete terms, the thin Bi_2Te_3 nanosheets may have incomplete quintuple layers (QLs) at the surface. Atoms on and near the surface will lose some neighbour atoms and electron density, possess higher energies and are more likely to move out of the plane and thus break the symmetry along the *c* axis and make the A_{1u} modes Raman active.[33] According to the reports about the Raman pattern of 2D crystals a few QL in thickness, the intensity of the A_{1u} peak and the intensity ratio $I(A_{1g}^2)/I(E_g^2)$ increases with decreasing thickness which can be used for

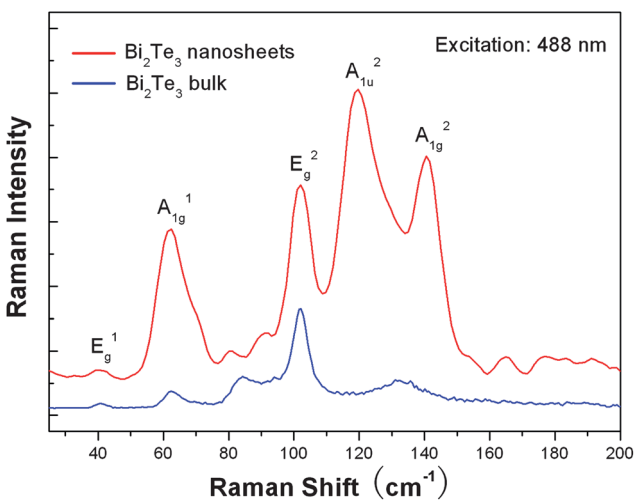

Fig. 4 Raman spectra of Bi_2Te_3 nanosheets and Bi_2Te_3 bulk, respectively.

Table 1 Raman bands in bulk Bi_2Te_3 and nanosheets

	E_g^1	A_{1g}^1	E_g^2	A_{1u}^2	A_{1g}^2	Ref.
bulk	40.7	62.5	102.3	—	132.4	this work
nanosheet	40.4	62.4	102.0	119.6	140.5	this work
bulk	40.2	60.2	100.8	—	133.2	33
2D	40.1	59.1	100.8	115.2	137.2	33
40 nm	38.9	61.3	107.3	116.2	133.0	31
4 nm	38.9	60.9	101.4	116.7	132.9	31

nanometrology of few-QL films.[31,34] For clear comparison, the assignment of the Raman bands from this work and literature is summarized in Table 1. Consequently, the investigations of Raman spectra indicate that the exfoliated films are crystalline and atomically thin.

To further confirm the thickness of as-prepared nanosheets, the AFM topography images of Bi_2Te_3 nanosheets are investigated. As shown in Fig. 5, most of the nanosheets have very clean and flat surfaces with a uniform thickness (~4 nm) across the lateral dimensions. The thickness distribution for Bi_2Te_3 is obtained by scanning a substrate area of ~5 × 5 μm^2 and the height profiles corresponding to the dashed line-cut are shown in the right frame. Large nanosheets with uniform thicknesses between 3 QLs and 4 QLs (3–4 nm) are major products (height profiles (i, ii)). An ultrathin TI structure down to a few (<5) nanometres is predicted to possess many exotic physical phenomena,[35,36] such as topologically nontrivial edge states which may serve as a new platform for the 2D quantum spin Hall effect. In view of that, the as-prepared Bi_2Te_3 with about 4 QLs and simply obtained thin films of Bi_2Te_3 are regarded as attractive for probing TI surface states and future device applications.

The former discussions corresponding to the Bi_2Te_3 bulk and the exfoliated Bi_2Te_3 nanosheets have provided insight into the procedure of this insertion/exfoliation method. The digital images (Fig. 6 (a)) provide the detailed statements about our process of intercalation and exfoliation. As shown schematically in Fig. 6 (b), we propose the formation of nanosheets from the solid state precursor occurs as follows. In the first step, lithium atoms are intercalated into the van der Waals bonded interlayers of Bi_2Te_3 during the hydrothermal procedure. The structure of bismuth telluride and its alloys can be considered as layers made up of 5 atom thick Te-Bi-Te-Bi-Te covalently bound sheets coupled together by much weaker van der Waals forces. In the presence of ethylene glycol which served as both reductant and solvent, the Li cations dissolve in the solvent and insert into Bi_2Te_3 to form $Li_yBi_2Te_3$ during the reduction process as given in eqn (1). After that, the Li-intercalated $Li_yBi_2Te_3$ powders are exposed to water to make the lithium ions in $Li_yBi_2Te_3$ rapidly become solvated and result in the production of lithium hydroxide (LiOH) and hydrogen gas. In eqn (2), original quintuple layers are homogeneously exfoliated due to the rapid expansion in the layers and forming suspensions of Bi_2Te_3 nanosheets. The powder of the Bi_2Te_3 nanostructure can be facilely obtained by filtration and it is also easy to deposit and dry to form two-dimensional films for potential application in next-generation quantum computing devices or thermoelectric devices.

$$Bi_2Te_3 + yLi^+ + ye^- \rightarrow Li_y^+(Bi_2Te_3)^{-y} \quad (1)$$

$$Li_yBi_2Te_3 + yH_2O \rightarrow Bi_2Te_3\ (\text{nano}) + yLiOH + \frac{y}{2}H_2\uparrow \quad (2)$$

To optimize the preparation conditions, we contrast the samples obtained by the hydrothermal at different temperatures. According to the SEM images of the samples, a gradual change from bulk Bi_2Te_3 to nanosheets is observed (see ESI,† Fig. S2). It is suggested that effective insertion can be only operated at or above a specific temperature. In our route of fabricating the Bi_2Te_3 nanosheets, it could be noted that ethylene glycol, as reductant and solvent, is regarded as essential for the intercalation process in the hydrothermal reaction. To illustrate this issue, we used LiOH dissolved in water as the hydrothermal solvent. The outcome of contrast tests indicated that the intercalation of Li ion in the Bi_2Te_3 bulk scarcely occurred in aqueous solution of LiOH in the hydrothermal process (see ESI,† Fig. S3 and S4). The reason for this phenomenon is ascribed to the rapid combination of lithium ions and water to form a hydrate and it is difficult for the hydrate to insert into the layers. Typically, the method we mentioned here requires both reductant and anhydrous solvent. Therefore, ethylene glycol would be a good

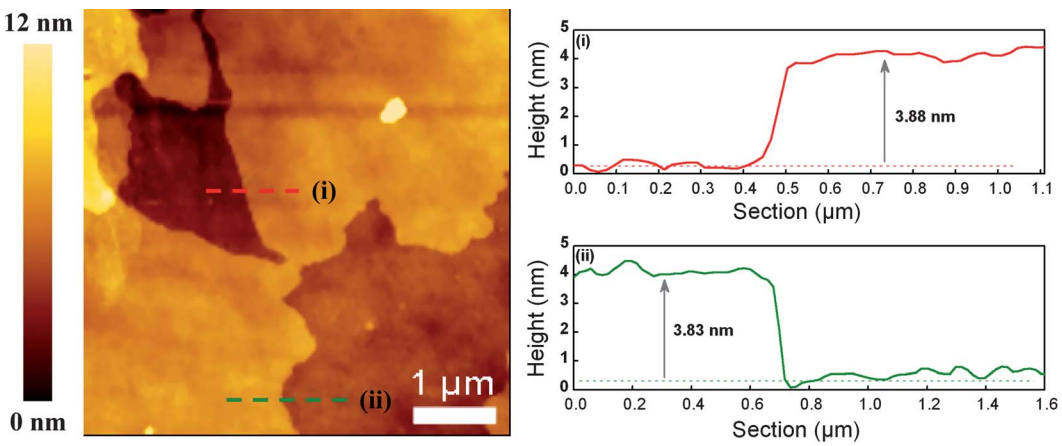

Fig. 5 Typical AFM image and height profiles (corresponding to the dashed lines in the image) of Bi_2Te_3 thin film.

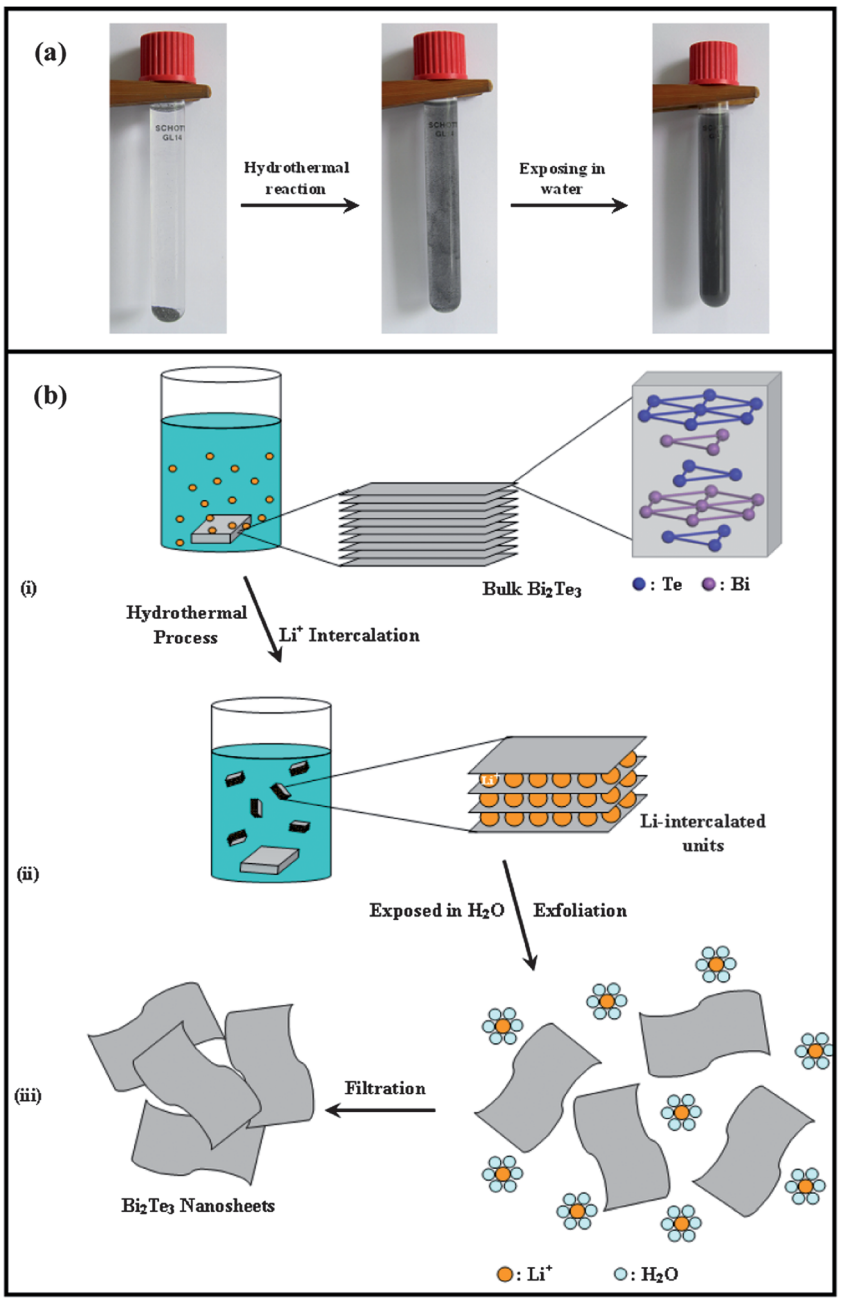

Fig. 6 Schematic representation of the formation of Bi_2Te_3 nanosheets.

candidate which can benefit greatly the intercalation of Li ions. Though ethylene glycol is an organic substance, fortunately it is easy to eliminate by rinsing with acetone. Furthermore, a pure and high quality Bi_2Te_3 nanosheets membrane can be obtained by filtration (see ESI,† Fig. S5). Thus, for potential applications, mass-produced Bi_2Te_3 nanosheets are practicable using this novel hydrothermal intercalation/exfoliation method. By the way, this exfoliation process is not limited to Bi_2Te_3, we have also successfully Li-inserted and exfoliated Bi_2Se_3 and MoS_2 (the SEM images are shown in Fig. S6). As it can be applied to the above-mentioned materials, we propose that this novel intercalation/exfoliation method is general and it is expected to extend to other layered compounds.

4. Conclusion

In summary, we demonstrate a novel method to intercalate lithium into Bi_2Te_3 using a common hydrothermal process. A large quantity of Bi_2Te_3 nanosheets were obtained after the resulting lithiated materials were exfoliated in water. These products have high purity with flat and smooth surfaces, and it is easy and flexible to achieve their migration onto substrates for further research. The whole process is energy-saving, and batch production can be achieved by further amplification of the intercalation devices. Therefore, this chemical intercalation and exfoliation may prove to be a simple and effective method for making two-dimensionally ordered bismuth telluride, which

should pave the way for room temperature spintronics applications and high efficiency thermoelectric devices.

Acknowledgements

We would like to thank Prof. Chunxu Pan and Dr Yupeng Zhang (Department of Physics, Wuhan University) for their excellent technical assistance on Raman spectra characterization. This work was supported by Grants from National Natural Science Foundation of China (Nos. 51172191, 51002129, 11074211, and 10802071), the Cultivation Fund of the Key Scientific and Technical Innovation Project (708068), Ministry of Education of China, the Doctoral Program of Higher Education (No. 200805300003) and the China Postdoctoral Science Foundation funded project (No. 20100480068).

References

1 B. L. Huang and M. Kaviany, *Phys. Rev. B: Condens. Matter Mater. Phys.*, 2008, **77**, 125209.
2 D. A. Wright, *Nature*, 1958, **181**, 834.
3 H. Zhang, C. X. Liu, X. L. Qi, X. Dai, Z. Fang and S. C. Zhang, *Nat. Phys.*, 2009, **5**, 438.
4 X. L. Qi and S. C. Zhang, *Phys. Today*, 2010, **63**, 33.
5 J. E. Moore, *Nature*, 2010, **464**, 194.
6 D. Hsieh, D. Qian, L. Wray, Y. Xia, Y. S. Hor, R. J. Cava and M. Z. Hasan, *Nature*, 2008, **452**, 970.
7 Y. L. Chen, J. G. Analytis, J. H. Chu, Z. K. Liu, S. K. Mo, X. L. Qi, H. J. Zhang, D. H. Lu, X. Dai, Z. Fang, S. C. Zhang, I. R. Fisher, Z. Hussain and Z. X. Shen, *Science*, 2009, **325**, 178.
8 Y. Xia, D. Qian, D. Hsieh, L. Wray, A. Pal, H. Lin, A. Bansil, D. Grauer, Y. S. Hor, R. J. Cava and M. Z. Hasan, *Nat. Phys.*, 2009, **5**, 398.
9 D. Hsieh, Y. Xia, D. Qian, L. Wray, J. H. Dil, F. Meier, J. Osterwalder, L. Patthey, J. G. Checkelsky, N. P. Ong, A. V. Fedorov, H. Lin, A. Bansil, D. Grauer, Y. S. Hor, R. J. Cava and M. Z. Hasan, *Nature*, 2009, **460**, 1101.
10 D. Kong, W. Dang, J. J. Cha, H. Li, S. Meister, H. Peng, Z. Liu and Y. Cui, *Nano Lett.*, 2010, **10**, 2245.
11 H. Peng, K. Lai, D. Kong, S. Meister, Y. Chen, X. L. Qi, S. C. Zhang, Z. X. Shen and Y. Cui, *Nat. Mater.*, 2010, **9**, 225.
12 F. Xiu, L. He, Y. Wang, L. Cheng, L. T. Chang, M. Lang, G. Huang, X. Kou, Y. Zhou, X. Jiang, Z. Chen, J. Zou, A. Shailos and K. L. Wang, *Nat. Nanotechnol.*, 2011, **6**, 216.
13 Y. Zhang, K. He, C. Z. Chang, C. L. Song, L. L. Wang, X. Chen, J. F. Jia, Z. Fang, X. Dai, W. Y. Shan, S. Q. Shen, Q. Niu, X. L. Qi, S. C. Zhang, X. C. Ma and Q. K. Xue, *Nat. Phys.*, 2010, **6**, 584.
14 Y. Y. Li, G. Wang, X. G. Zhu, M. H. Liu, C. Ye, X. Chen, Y. Y. Wang, K. He, L. L. Wang, X. C. Ma, H. J. Zhang, X. Dai, Z. Fang, X. C. Xie, Y. Liu, X. L. Qi, J. F. Jia, S. C. Zhang and Q. K. Xue, *Adv. Mater.*, 2010, **22**, 4002.
15 J. J. Cha, J. R. Williams, D. Kong, S. Meister, H. Peng, A. J. Bestwick, P. Gallagher, D. Goldhaber-Gordon and Y. Cui, *Nano Lett.*, 2010, **10**, 1076.
16 D. Kong, J. C. Randel, H. Peng, J. J. Cha, S. Meister, K. Lai, Y. Chen, Z. X. Shen, H. C. Manoharan and Y. Cui, *Nano Lett.*, 2009, **10**, 329.
17 K. S. Novoselov, A. K. Geim, S. V. Morozov, D. Jiang, Y. Zhang, S. V. Dubonos, I. V. Grigorieva and A. A. Firsov, *Science*, 2004, **306**, 666.
18 D. Teweldebrhan, V. Goyal and A. A. Balandin, *Nano Lett.*, 2010, **10**, 1209.
19 D. Teweldebrhan, V. Goyal, M. Rahman and A. A. Balandin, *Appl. Phys. Lett.*, 2010, **96**, 053107.
20 M. Z. Hossain, S. L. Rumyantsev, K. M. F. Shahil, D. Teweldebrhan, M. Shur and A. A. Balandin, *ACS Nano*, 2011, **5**, 2657.
21 M. Z. Hossain, S. L. Rumyantsev, D. Teweldebrhan, K. M. F. Shahil, M. Shur and A. A. Balandin, *Phys. Status Solidi A*, 2011, **208**, 144.
22 J. N. Coleman, M. Lotya, A. O'Neill, S. D. Bergin, P. J. King, U. Khan, K. Young, A. Gaucher, S. De, R. J. Smith, I. V. Shvets, S. K. Arora, G. Stanton, H. Y. Kim, K. Lee, G. T. Kim, G. S. Duesberg, T. Hallam, J. J. Boland, J. J. Wang, J. F. Donegan, J. C. Grunlan, G. Moriarty, A. Shmeliov, R. J. Nicholls, J. M. Perkins, E. M. Grieveson, K. Theuwissen, D. W. McComb, P. D. Nellist and V. Nicolosi, *Science*, 2011, **331**, 568.
23 Z. Zeng, Z. Yin, X. Huang, H. Li, Q. He, G. Lu, F. Boey and H. Zhang, *Angew. Chem., Int. Ed.*, 2011, **50**, 11093.
24 J. Bludská, S. Karamazov, J. Navrátil, I. Jakubec and J. Horák, *Solid State Ionics*, 2004, **171**, 251.
25 I. D. Koz'mik, I. I. Grigorchak, Z. D. Kovalyuk, B. P. Bakhmatyuk, S. V. Gavrilyuk and M. V. Tovarnitskii, *Russ. J. Phys. Chem.*, 1990, **64**, 840.
26 S. N. Chizhevskaya, T. E. Svechnikova, S. Y. Skipidarov, N. A. Tsvetkova and N. N. Nemtsov, *Inorg. Mater.*, 1992, **28**, 231.
27 Z. Ding, L. Viculis, J. Nakawatase and R. B. Kaner, *Adv. Mater.*, 2001, **13**, 797.
28 Z. Ding, S. K. Bux, D. J. King, F. L. Chang, T. H. Chen, S. C. Huang and R. B. Kaner, *J. Mater. Chem.*, 2009, **19**, 2588.
29 W. Richter and C. R. Becker, *Phys. Status Solidi B*, 1977, **84**, 619.
30 V. Russo, A. Bailini, M. Zamboni, M. Passoni, C. Conti, C. S. Casari, A. Li Bassi and C. E. Bottani, *J. Raman Spectrosc.*, 2008, **39**, 205.
31 K. M. F. Shahil, M. Z. Hossain, D. Teweldebrhan and A. A. Balandin, *Appl. Phys. Lett.*, 2010, **96**, 153103.
32 J. M. Friedman and R. M. Hochstrasser, *J. Am. Chem. Soc.*, 1976, **98**, 4043.
33 Y. Zhao, R. W. Hughes, Z. Su, W. Zhou and D. H. Gregory, *Angew. Chem., Int. Ed.*, 2011, **50**, 1.
34 V. Goyal, D. Teweldebrhan and A. A. Balandin, *Appl. Phys. Lett.*, 2010, **97**, 133117.
35 B. Seradjeh, J. E. Moore and M. Franz, *Phys. Rev. Lett.*, 2009, **103**, 066402.
36 C. X. Liu, H. Zhang, B. Yan, X. L. Qi, T. Frauenheim, X. Dai, Z. Fang and S. C. Zhang, *Phys. Rev. B: Condens. Matter Mater. Phys.*, 2010, **81**, 041307.

